

LADFN: Learning Actions for Drift-Free Navigation in Highly Dynamic Scenes

Mohd Omama¹, Sundar Sripada V. S.¹, Sandeep Chinchali², and K. Madhava Krishna¹

¹Robotics Research Center, IIIT-Hyderabad

²ECE Department, The University of Texas at Austin

Abstract—We embark on a hitherto unreported problem of an autonomous robot (self-driving car) navigating in dynamic scenes in a manner that reduces its localization error and eventual cumulative drift or Absolute Trajectory Error, which is pronounced in such dynamic scenes. With the hugely popular Velodyne-16 3D LIDAR as the main sensing modality, and the accurate LIDAR-based Localization and Mapping algorithm, LOAM, as the state estimation framework, we show that in the absence of a navigation policy, drift rapidly accumulates in the presence of moving objects. To overcome this, we learn actions that lead to drift-minimized navigation through a suitable set of reward and penalty functions. We use Proximal Policy Optimization, a class of Deep Reinforcement Learning methods, to learn the actions that result in drift-minimized trajectories. We show by extensive comparisons on a variety of synthetic, yet photo-realistic scenes made available through the CARLA Simulator the superior performance of the proposed framework vis-à-vis methods that do not adopt such policies.

Index Terms—Active Navigation, Deep Reinforcement Learning, Proximal Policy Optimization, LIDAR Odometry and Mapping, Stanley Controller, Absolute Pose Error.

I. INTRODUCTION

With rapidly increasing popularity of self-driving vehicles, there is a growing need for their adroit maneuvering in highly dynamic scenes, not only from the point of view of collision avoidance, but also from the point of view of drift-minimal navigation, which particularly takes a hit in the presence of several moving objects. Highly dynamic scenes pose specific challenges as the signal is buried in noise for any kind of sensor based localization/state estimation methods to prove effective. The autonomous vehicle needs to actively modify its behavior and navigation actions, often searching for spaces to move into from where it can reduce its drift and enhance its state estimation accuracy. To the best of our knowledge, there seems no literature that tackles this problem head on.

In this paper, we present a novel active localization framework that seeks and learns actions that lead to and result in drift-minimized navigation in the presence of dynamic obstacles, as shown in Figure 1. By suitably-crafted reward functions and PPO [3] as its Deep Reinforcement Learning architecture, action policies are learned that achieve this cause. We show by extensive comparisons in a variety of dynamic scenes the efficacy and superiority of this architecture in achieving drift-minimized navigation vis-à-vis methods that do not actively navigate to minimize state estimation errors.

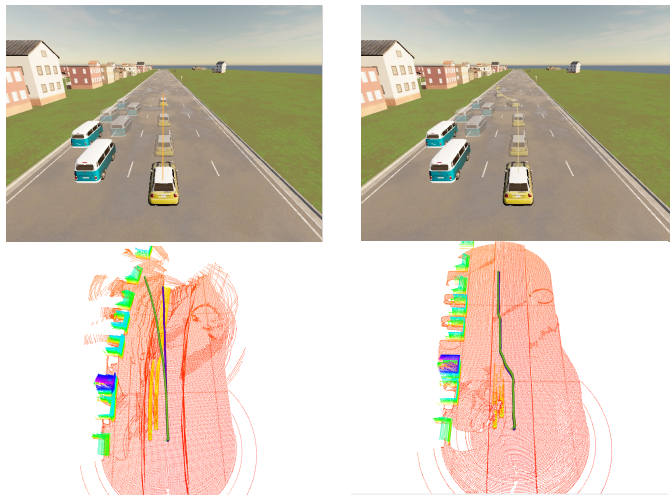


Fig. 1: Active navigation significantly reduces autonomous vehicle drift. Left column represents baseline (Stanley Control) and right column represents our approach (LADFN). **Top Panel:** CARLA [1] environments showing ego vehicles planning their trajectories. **Bottom Panel:** LOAM [2] map visualizations of the same scenes. The green lines delineate ground-truth trajectories, and the purple lines delineate LOAM’s generated odometry. While drift from the green ground-truth is pronounced on the left, with LADFN there is no such drift or deviation on the right. For a **100m** run, a Stanley-controlled ego drifts in the xy -plane by **14.05m**, eventually colliding with nearby traffic, whereas an ego controlled by our approach drifts by **0.62m**, due to traffic collision-avoidance and active navigation towards nearby features. This drift also affects LOAM’s [2] mapping potential: the map on the left is distorted due to the ego’s haphazard odometry, whereas the map on the right remains relatively unaffected.

A pivotal contribution of this work is to showcase the need for active navigation for minimizing drift that goes beyond popular filtering approaches that filter measurements due to dynamic actors to improve state estimation accuracy. However, in many instances, filtering dynamic actors is only partially helpful. It is equally, if not more, important to adapt an active localization strategy that learns to navigate to minimize drift in presence of dynamic objects. We depict this main novelty extensively through comparisons with filtering approaches to state estimation in a variety of CARLA Scenes with high traffic in various lanes. Henceforth, we call our system **LADFN** - **L**earning **A**ctions for **D**rift-**F**ree **N**avigation. And for notational convenience, we refer to our autonomous vehicle as *ego vehicle* or *ego* interchangeably.

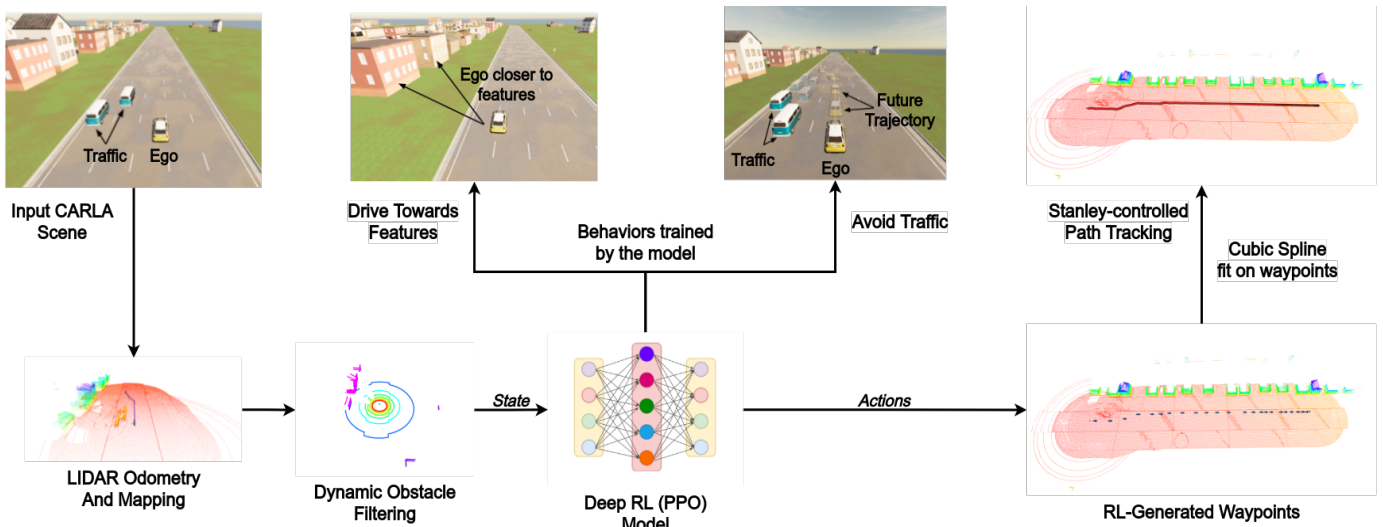


Fig. 2: **Pipeline of our approach.** First, a map of the input CARLA [1] scene is built using LOAM [2]. Filtering is applied to remove dynamic traffic objects, if present. The state obtained from this map is passed into a deep RL neural network that performs Proximal Policy Optimization [3], to help choose actions $a \in \mathcal{A}$, our action space. This model ensures that the ego drives towards feature-rich lanes and avoids traffic in its way. The action inferences from the model are then used to generate a set of discrete waypoints for the ego to traverse. A cubic spline is fit on these waypoints to generate a smooth trajectory, which is then tracked using a Stanley Controller [4].

A. Related Work

State estimation or localization that involves computing the pose of the robot comes in various flavors with different sensing modalities such as those that estimate both the agent’s motion and the map [5], [6], or those that only estimate the agent’s motion or odometry [2], [7]. Prominent amongst these include the highly popular LOAM [2] and its variants [8], with LIDAR as the primary sensing modality or vision-based frameworks with or without direct availability of depth information [7], [9], [10]. A modest portion of this literature is devoted towards handling dynamic actors. Herein, the popular theme is about filtering dynamic obstacles to enhance estimation accuracy irrespective of the sensing modality [11]–[16]. For example, authors in [17] proposed to detect and eliminate the dynamic regions using a sparse motion removal (SMR) based on similarity and difference between frames that is fed to a Bayesian framework for motion detection and filtering. While [12] used background segmentation methods to filter dynamic agents, [13] used ego-motion compensation to detect dynamic regions in the current frame with subsequent vector quantization to segment moving regions in the scene. Other methods such as [18], [19] jointly estimate stationary and moving agents in a multi-body framework. Amongst the popular LIDAR based frameworks, [20] use long term mapping techniques to segment moving parts of the scene, while the stationary parts of the scene are used for localization and the moving agents are maintained in the map in the form of their velocity representations. In [21], a distance-filtering approach is utilized to segment the dynamic contents of the scene while maintaining stationary parts as raw pointclouds.

The field of active localization, or actively navigating the robot or the ego to minimize localization errors, has received

some attention in the literature. Active localization was popularized due to [22], [23] in their own ways. While [22] focused on actively navigating towards less-aliased regions in the scene so as to converge towards a unimodal estimate of the state from a multi-modal belief due to perceptual aliasing, the main theme in [23] was actively navigating to reduce the uncertainty of the unimodal state distribution. The complexity of active localization was analyzed in [24] and was shown to be NP-Hard, whereas a randomized algorithm for the same was presented in [25]. The first and possibly only such formulation for active localization in a multi-agent setting was presented in [26]. However, none of the active frameworks talk of navigating an agent to reduce drift in the presence of moving agents.

This work distinguishes itself from all the prior art in several ways. For one, it is the first such method to tackle the problem of active navigation in dynamic on-road scenes. In contrast to the state estimation approaches, the present formulation showcases the need to go beyond filtering frameworks by learning actions to maneuver around dynamic actors in a manner that reduces drift. Unlike previous methods for active navigation that only handled stationary scenes, the current formulation is specifically tailored towards highly dynamic on-road scenes.

II. PIPELINE FLOW

The complete end-to-end architecture of LADFN is shown in Figure 2. We now describe the implementation detail of each of these modules:

- 1) *Perception and Dynamic Obstacle Filtering*: We use an out-of-the-box implementation of LOAM [2]. Then, we filter LIDAR points originating from traffic vehicles.
- 2) *Waypoint Generation*: We use an RL model to choose actions that provide discrete waypoints for the ego to

traverse. The model is unrolled for n steps to get a trajectory.

- 3) *Trajectory Interpolation*: We fit a cubic spline on the trajectory to smoothen it.
- 4) *Low-level Control*: We use a Stanley Controller [4] to perform path tracking on the trajectory.

A. Perception and Dynamic Obstacle Filtering

LIDAR Odometry and Mapping (LOAM) [2] is a SLAM technique [27] developed for 3D LIDAR sensors. LOAM splits the complex problem of optimizing several thousand variables simultaneously by splitting the mapping and localizing procedures into two: *laser odometry* and *laser mapping*. *Laser odometry* runs at a high frequency and seeks to localize the LIDAR by calculating its velocity in every frame. *Laser mapping* runs at a lower frequency and finds edge-edge correspondences and plane-plane correspondences. These two processes are followed by iterative scan matching to get the translation T and rotation R . LOAM is a state-of-the-art odometry solution on several benchmark datasets, especially KITTI [28]. In our method, LOAM runs in the background interacting with the LIDAR points originating from CARLA. We use CARLA's [1] provided LIDAR segmentation to filter out points coming from dynamic vehicles and test our approach both in the presence and absence of this filtering. The odometry output from LOAM is piped into the waypoint generation module, discussed in detail in Section II-B.

B. Waypoint Generation

The Waypoint Generation problem will be formulated as a Markov Decision Process (MDP) in Section III. While there are a plethora of deep RL algorithms to approximately solve this MDP, we chose PPO [3] since it is well-established and well-suited for discrete action spaces that our setting requires. We also note that the primary novelty of our paper is the MDP formulation for active navigation to reduce drift, and other RL algorithms should perform well in practice. For both the actor and the critic, we have a fully connected network with 6 hidden layers. The number of neurons in each hidden layer are: 64, 64, 32, 32, 16 and 16 respectively. We use ReLU activation along with a batch-size of 128 and a discount factor γ of 0.9999. Our architecture conforms to the implementation of PPO in Stable-Baselines 3 [29].

We synthetically create a wide range of initial states. These states span across multiple combinations of ego positions, traffic positions, traffic speeds, positions of centroid of edge features, etc., During training, we assume that the position of centroid of edge features remains constant for that episode. This hypothesis is valid because our training episodes last for only 10 steps. We created an environment that takes as input at time t the state s_t , and the action a_t , and outputs at time $t + 1$ the next state s_{t+1} , and reward r_{t+1} . This environment was used to train an RL agent without directly interacting with the CARLA [1] Simulator. The episode is terminated either at the completion of 10 steps, or when the ego breaches lane boundaries, or when the ego collides with the traffic.

C. Trajectory Interpolation

The waypoints obtained from PPO are then passed into a cubic spline planner for interpolation in order to obtain a smooth trajectory that our ego can traverse. During inference, we unroll the waypoint generation module n times to get an n -step trajectory. We then fit a cubic spline on it using an existing framework provided by Sakai *et al.* [30].

D. Low-level Control

The final step in our process is to traverse the smooth spline and ensure that the ego is tracking the path with minimal drift. For this purpose we use a standard Stanley Controller [4], but it should be noted that our approach is invariant to the choice of the path tracking algorithm. The implementation of Stanley used is also provided by Sakai *et al.* [30].

III. MODEL-FREE RL FOR DRIFT MINIMIZATION

Reinforcement Learning (RL) has been extensively used to solve a vast variety of Markov Decision Processes (MDPs). A canonical MDP comprises of a state space \mathcal{S} , an action space \mathcal{A} , a transitional probability, $\mathcal{P}: \mathcal{S} \times \mathcal{A} \times \mathcal{S} \rightarrow [0, 1]$, that governs the transition from state s_t to state s_{t+1} , a reward function, $\mathcal{R}: \mathcal{S} \times \mathcal{A} \times \mathcal{S} \rightarrow \mathbb{R}$, which describes a scalar reward that is associated with the transition from state s_t to s_{t+1} by taking an action a_t , and a discount factor γ which controls the importance we give to future rewards. When we solve the MDP, we find a policy $\pi: \mathcal{S} \rightarrow \mathcal{A}$, such that it maximises the value function V_π :

$$V_\pi(s_0) = \mathbb{E} \left(\sum_{t=0}^{\infty} \gamma^t \mathcal{R}(s_{t+1}, s_t, \pi(s_t)) \right), \quad (1)$$

Now, we will formulate LADFN's waypoint generation problem as an MDP and provide a detailed account of the state space \mathcal{S} , the action space \mathcal{A} and the reward \mathcal{R} . The dynamics of our MDP depend on the motion of the ego-vehicle as well as the uncontrolled motion of other traffic. Specifically, we cannot analytically model where other traffic will move, nor what the ego will observe at future time-steps from its LIDAR sensors. Since we do not have an analytical model for the full dynamics of the MDP, we resort to model-free deep RL to solve for a control policy. We first define a frame whose X -axis points along the direction of the road, and whose Y -axis is perpendicular to the direction of the road. The ego's starting coordinate in this frame will be of the form $(0, y_e)$. We refer to this frame as the *RL frame* (Figure 3).

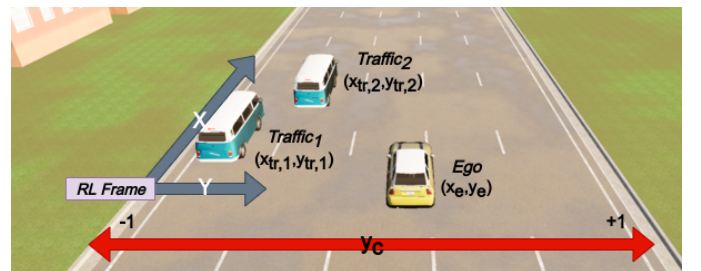


Fig. 3: Our *RL Frame* representation in a CARLA scene.

A. State

We define the state of the RL agent as a vector such that it captures all necessary task-relevant information. The entries of the state space vector will be in *RL frame* unless stated otherwise. The state vector is as follows:

- x_e : x-coordinate of ego vehicle
- y_e : y-coordinate of ego vehicle
- y_c : y-coordinate of centroid of the edge features which is clipped and scaled to $[-1, 1]$; edge features are discussed in Section III-C
- $edge_l$: left limit of the road
- $edge_r$: right limit of the road
- tr_{p_i} : Boolean representing the presence of i^{th} traffic vehicle
- x_{tr_i} : x-coordinate of the i^{th} traffic vehicle
- y_{tr_i} : y-coordinate of the i^{th} traffic vehicle
- v_{tr_i} : velocity of the i^{th} traffic vehicle.

B. Action Space

The RL agent has a set of discrete actions \mathcal{A} that it can choose from. Each action $a \in \mathcal{A}$, represents the waypoint at the next time step for the vehicle in the vehicle's frame of reference. The action a is defined as a tuple (a_x, a_y) where $a_x \in \{1, 2, 3, 5\}$ represents x -coordinate of the next waypoint, and $a_y \in \{-2, -1, 0, 1, 2\}$ represents y -coordinate of the next waypoint in the vehicle's frame. We ensured that our action space reflects a spectrum of ways in which the vehicle could move: from slow-straight motion to fast-turning motion.

C. Motivation For Reward Shaping

LOAM [2] geometrically categorizes the LIDAR points as edge or plane features which are then used in scan-matching. Edge features represent texture-rich regions which help in accurate scan-matching. We will refer to such regions as *feature-rich*. In order to sustain LOAM's [2] map-building process, and more importantly, reduce the absolute pose error (APE) in ego-motion, the first consideration is the ego's proximity to feature-rich regions. This can be argued as follows.

Consider two vehicles ego_1 and ego_2 and a feature-rich region T_R as shown in Figure 4, where ego_1 is closer to T_R than ego_2 . We draw tangents from the two vehicles to T_R . Let the angles that these two sets of tangents subtend with T_R be θ_1 and θ_2 respectively. Also, consider a planar LIDAR which has a 360° field view of a single plane and an angular resolution of n . The number of LIDAR rays per unit angle will then be $\frac{n}{360}$. Now, the number of LIDAR rays that interact with the feature-rich region in both the cases will be $\frac{n \times \theta_1}{360}$ and $\frac{n \times \theta_2}{360}$ respectively. Since, ego_1 is closer to T_R than ego_2 , θ_1 will be larger than θ_2 , indicating that more LIDAR rays will interact with T_R in the first case leading to its more dense reconstruction. The same argument can be extended for 3D LIDAR which is the primary hardware setting in our proposed solution. Therefore, when the ego is in the proximity of texture-rich regions, LOAM can more densely reconstruct them since the incoming pointcloud to LOAM will have more edge features contained in it.

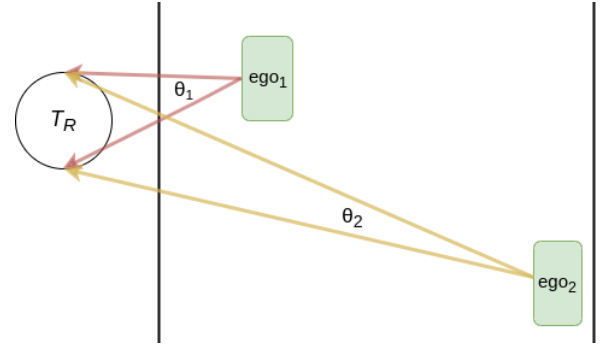


Fig. 4: **Benefits of active navigation towards feature-rich regions.** More LIDAR rays from ego_1 than ego_2 interact with the texture-rich region T_R , since $\theta_1 > \theta_2$, resulting in a more dense reconstruction.

The second aspect that plays an impact on the APE is the distance from traffic vehicles. LIDAR points from dynamic objects lead to erroneous registrations in the scan-matching algorithm; in our case, the dynamic objects are said traffic vehicles. Further, proximity to dynamic vehicles can also occlude visibility of other texture-rich regions. Follow-up papers [31], [32] on LOAM have argued the same. Further, Thomas *et al.* [31], have specifically shown that the proximity to dynamic vehicles leads to substantial error in the rotational measurement, R . Our experimentation in dynamic scenes also resonates with the findings of these works but unlike us, none of them address drift-minimizing behaviors.

To handle the problems described above, the ego should be aware of the feature-rich regions and plan its trajectory accordingly. It should also avoid proximity with traffic wherever possible. Our proposed solution comprises of an RL agent that generates waypoints which are then traversed with the aid of a low-level controller. The input to the RL agent is a state that includes the centroid of edge features, the ego's pose, and the traffic vehicles' poses. We calculate the centroid using queried edge features obtained through LOAM. The pose of the ego is directly queried from LOAM. We also assume that we have the speed and pose information of the traffic readily available due to recent advancements in LIDAR-based semantic segmentation and tracking [33].

D. Reward

The reward was designed with two primary objectives: navigation and perception. The navigation objectives comprise of the follows.

- 1) Forward motion: We incentivize the ego to move forward towards the goal.
- 2) Road boundary constraint: $edge_l \leq y_e \leq edge_r$, i.e., the ego should move within the road boundaries.
- 3) Collision constraint: $\|(x_{tr_i}, y_{tr_i}) - (x_e, y_e)\| \geq 3$ meters, i.e., the ego must not collide with the traffic.

The perception objectives comprise of the follows.

- 1) Feature proximity: *minimize* $|y_e - y_c|$, i.e., the ego should try to maintain proximity with the feature-rich regions.
- 2) Traffic distance: $\|(x_{tr_i}, y_{tr_i}) - (x_e, y_e)\| \leq 10m$, where the ego should try to avoid proximity with traffic.

Our reward \mathcal{R} models both the objectives described above and is defined as:

$$\mathcal{R} = \mathcal{P} \times \mathcal{T} + (1 - \mathcal{P}) \times \mathcal{F} + \mathcal{G}, \quad (2)$$

where $\mathcal{P} = \vee p_i$, which is the logical OR over all the *traffic-proximity* Boolean p_i . p_i will be described in detail in the *Traffic Reward* section. We now explain the other three terms in equation (2).

1) *The Goal Reaching Reward, \mathcal{G}* : \mathcal{G} returns a positive reward for forward motion along the X -axis towards the goal. Although a simple term, this ensures that the ego prioritizes moving towards the finish line besides pursuing feature-rich regions and avoiding traffic. The other navigation constraints like traffic and road limits are also modeled here. The ego is penalized if it collides with the traffic or moves out of the road, and the episode terminates.

2) *The Feature Reward, \mathcal{F}* : The feature reward needs to be shaped in a way that the ego is rewarded if it maintains proximity with feature-rich regions. To achieve this, we need two behaviors that are captured in two terms in (3) as follows:

a) *The first term*: The ego should move towards the left if the left side of the road is feature-rich and vice-versa. The lateral position of the feature-rich region is described by y_c , which is clipped and scaled to a normalized range of $[-1, 1]$. A value of -1 means the centroid of features is towards the left end of the road, and a value of 1 means the centroid is towards the right. To formulate the feature reward, we also need y_e in the range $[-1, 1]$. The term $(2((y_e - y_{e_{\min}})/(y_{e_{\max}} - y_{e_{\min}})) - 1)$ handles that. We first raise y_c to an odd power, O , and then multiply it with normalized y_e . This means that the reward will be positive if both y_c and normalized y_e have the same sign, implying they are on the same side of the road; and the reward will be negative if they are on the opposite sides of the road. Further, y_c^O forces the term following it to quickly drop to 0 when y_c is close to 0, ensuring that this *first term* has no impact when there are feature-rich regions on both sides of the ego.

b) *The second term*: If there are features on both sides of the road, the ego must prevent unnecessary lateral motion. To achieve this, we multiply the absolute of our lateral motion $|a_y|$ with $(1 - |y_c^O|)$. In this case, $|y_c^O|$ will be close to zero since features are on both sides and $(1 - |y_c^O|)$ will tend to 1. Further, $(1 - |y_c^O|)$ drops to zero when y_c is close to 1, ensuring that this second term has no impact when there are features on only one side of the road (left or right).

The complete mathematical formulation of the feature reward is given by:

$$\mathcal{F} = K_1 \times \left(y_c^O \times \left(\frac{2 \times (y_e - y_{e_{\min}})}{y_{e_{\max}} - y_{e_{\min}}} \right) - 1 \right) - K_2 \times (1 - |y_c^O|) \times |a_y|, \quad (3)$$

where K_1 and K_2 are constants.

3) *The Traffic Reward, \mathcal{T}* : We define a *traffic-proximity* region $\|(x_{tr_i}, y_{tr_i}) - (x_e, y_e)\| \leq 10m$ where the effect of traffic is large on localization. The traffic reward should be formulated such that the ego tries to move out of this region.

We design a reward which incentivizes the ego if the relative difference in forward direction between the ego and the traffic increases. It also returns a positive reward if the ego increases its lateral distance with the traffic car, and a negative reward otherwise. The traffic reward can be mathematically written as:

$$\mathcal{T} = \sum_{i=1}^n p_i \left[(K_3 \times |a_x - v_{tr_i}|) + K_4 \times (|y_{tr_i}^t - y_e^t| - |y_{tr_i}^{t-1} - y_e^{t-1}|) \right], \quad (4)$$

where p_i is a Boolean which is 1 only when the ego is in a *traffic-proximity* region, otherwise this traffic-vehicle has no impact on the reward, and K_3 and K_4 are constants. The summation term outside accumulates the rewards/penalties from each traffic vehicle i .

The waypoint generation MDP is solved using deep RL using an architecture described in Section II-B. We now evaluate our RL-based active navigation framework, LADFN, in challenging autonomous driving scenarios.

IV. EXPERIMENTS

This section begins with the description of our experimental setup, followed by a detailed qualitative and quantitative analysis of our approach in a wide array of realistic scenes.

A. Experimental Setup

The performance of LIDAR odometry algorithms can depend a lot on the physics of the environment as well as that of the ego. Hence, we use CARLA simulator [1] for our experimentation as it emulates real-world physics accurately. It is also a state-of-the-art high-fidelity simulation environment for autonomous driving and so it is ideal for our application. We simulate a 3D LIDAR in CARLA with 16 channels and a vertical field of view of 30° (-15° to 15°). The LIDAR emits 300,000 points per second which are evenly distributed over all channels. While running our experiments, we use three different LIDAR ranges: 45m, 50m, and 55m. These ranges correspond to the the maximum distance that can be measured by the LIDAR. The variety of LIDAR ranges during the experiments helps us analyze the performance of our method for various sensor ranges.

B. Scene Description

We have created a test bed of 5 different scenes in CARLA [1]. These scenes have a run length ranging from 100 to 500 meters, and include static as well as dynamic scenarios. We have created the scenes such that they have varying distributions of feature-rich regions and dynamic vehicles. Scenes 1 and 4 are static and don't have any dynamic traffic actors whereas scenes 2, 3 and 5 contain moving traffic cars or vans around the ego.

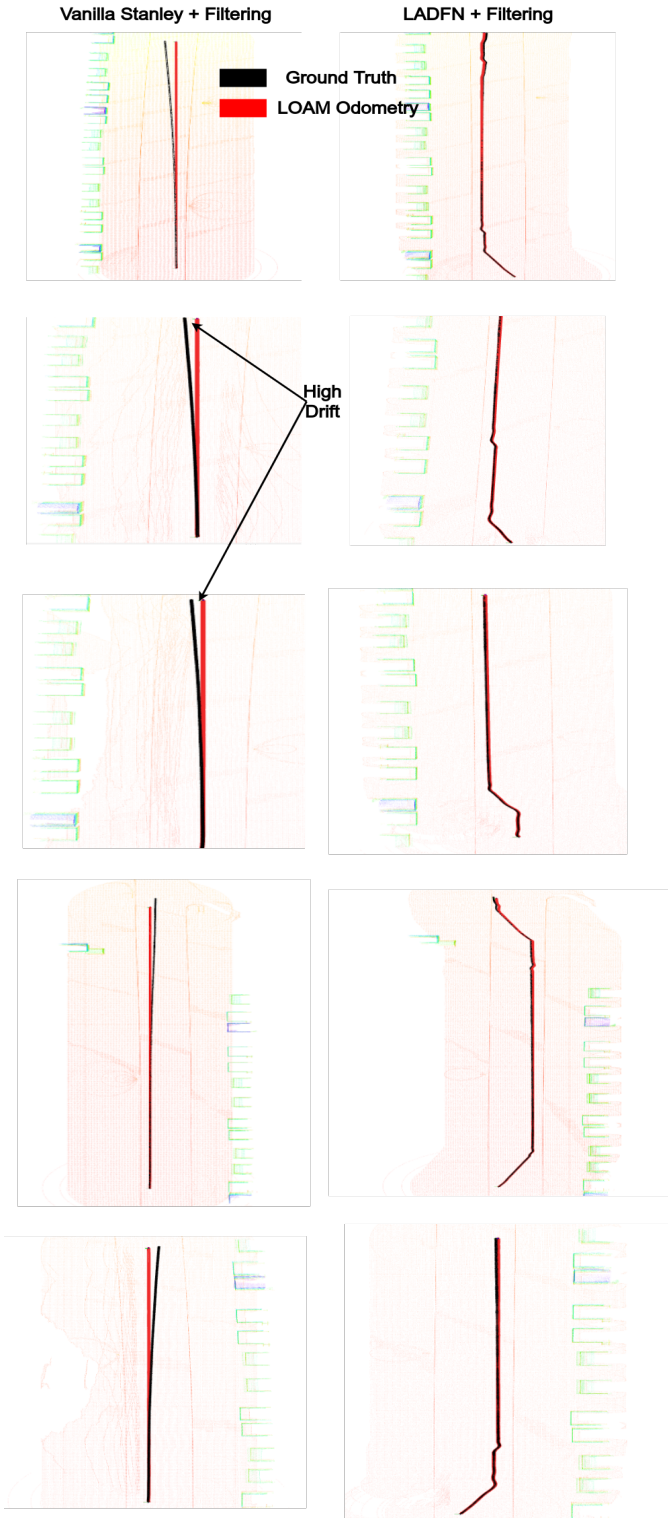


Fig. 5: LADFN significantly reduces drift with a minor change in the path taken to reach the goal. The LOAM-generated trajectories are shown in red, the ground-truth trajectories are shown in black, and the green structures correspond to feature-rich regions. The left column shows *Vanilla Stanley + F* while the right column shows *LADFN + F*. Each row corresponds to a different scene. These scenes were run with a LIDAR range of 45 meters and dynamic obstacle filtering enabled.

C. Metrics and Benchmarks

We benchmark our approach against what we call the *Vanilla Stanley Controller*. With *Vanilla Stanley*, the ego will not actively change its direction or speed to account for drift minimization. The ego will drive with a speed that is similar to the traffic around it. Hence, it represents *perception-unaware control*, a realistic scenario where the ego is tracking a trajectory without having any idea of the perception goals.

In dynamic scenes, a general approach to decrease trajectory error is to filter out dynamic vehicles from the LIDAR scans. Hence we have another benchmark which we refer to as *Vanilla Stanley + F* which is just a *Vanilla Stanley Controller* running with filtering enabled. We test and compare our proposed approach both in the presence and absence of dynamic obstacle filtering. This helps us understand that even when filtering is available, active navigation is essential to further reduce drift in the trajectory.

We use three different metrics for evaluating our approach:

- 1) *Average Drift*: The average translation drift in xy -plane for the entire trajectory.
- 2) *Final Drift*: Final translation drift in xy -plane at the end of the trajectory.
- 3) *Rotational Offset*: Yaw offset with respect to the ground-truth yaw at the goal location.

Metric 1 gives a general idea of the quality of localization achieved for the entire trajectory. *Metric 2* gives an idea of how the methods will perform on goal-reaching tasks. *Metric 3* serves two purposes: like *Metric 2*, this is also a representation for goal-reaching tasks, and further, it gives an idea of the quality of the future trajectory, since rotational errors in odometry have a compounding effect on the future trajectory.

D. Qualitative Results

Figure 5 shows a qualitative view of the trajectory and drift in all the five scenes. In the right column, as the estimated LOAM trajectory in red overlaps the ground-truth trajectory in black, unlike the baseline shown in the left column where the red deviates from the black, it can be clearly seen that with our approach, the drift is substantially reduced in every case. We can see that the ego tries to maintain proximity with the feature-rich regions shown in green. Rows 2, 3, and 5 correspond to dynamic scenes with filtering enabled and so traffic vehicles are not visible in the LIDAR scans shown in the Figure 5. We observe that even in the presence of filtering, our approach outperforms the baseline, highlighting the need for active navigation in drift minimization.

We achieve this due to the complex behaviours learned by our model, the examples of which can be seen in the following link: <https://mohdomama.github.io/LADFN/>. We show these in an external website due to brevity of space in the manuscript.

E. Quantitative Results

We depict the quantitative comparisons of our approach with the baselines in the five rows of Figure 6 corresponding to the five scenes. Rows 1 and 4 do not have dynamic

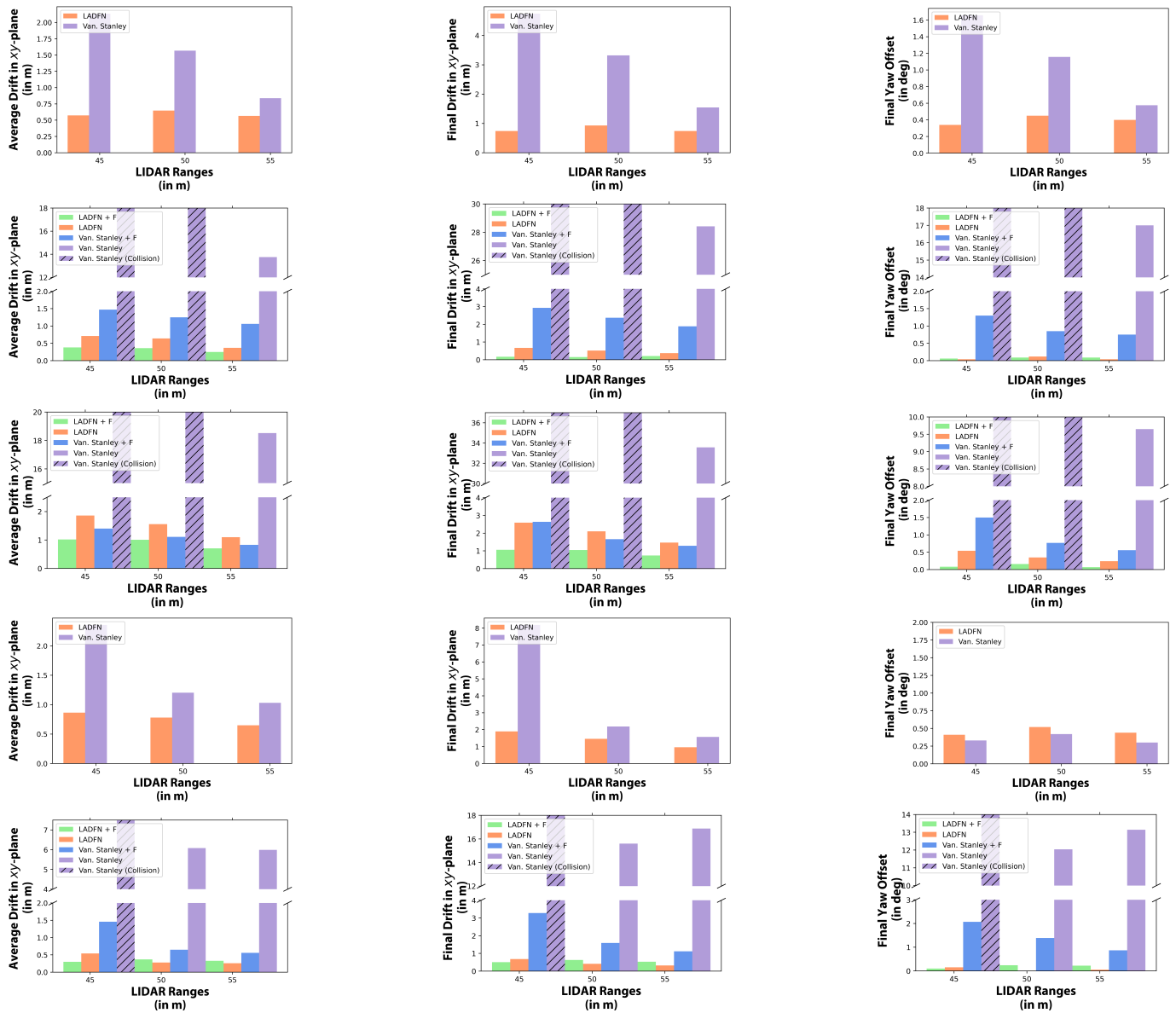


Fig. 6: LADFN significantly reduces drift than competing benchmarks on a diversity of CARLA scenes. Firstly, we want to show that LADFN leads to lower average drift than the benchmark. This is clearly shown in the **first column** where LADFN reduces Stanley’s drift by at least $1.48\times$. Secondly, we provide a framework for analyzing the performance of goal-reaching tasks, seen in the final translation offset plots in the **second column**, where once again, LADFN consistently outperforms the Vanilla Stanley controller by at least $1.63\times$. Thirdly, we show that rotational errors are significantly reduced by LADFN in the **third column**. In dynamic scenes (2,3,5), dynamic obstacle filtering was enabled. In **all** columns, *F* in the plot legends denotes that filtering of dynamic obstacles was carried out. Diagonal hatches ‘/’ inside bars represent collision occurrence of the ego with its surroundings in the experiment.

actors, and the comparison is between *LADFN* and *Vanilla Stanley*, shown with orange and violet bars. Rows 2, 3 and 5 correspond to the scenes populated with dynamic actors. Here, we include the filtering module in both the Stanley Controller and LADFN, denoted as *LADFN + F* and *Vanilla Stanley + F*, and shown with green and blue bars. In some scenes, the LOAM estimates have significantly deviated resulting in collision for the baseline *Vanilla Stanley*, these are shown with hatched violet bars.

Our first step is to show that LADFN leads to a lower average drift than benchmark competitors. This is clearly

shown in column 1. In static scenes, we get up to $3.7\times$ improvement in average drift using LADFN. In dynamic scenes, with filtering enabled, we get up to $4.8\times$ improvement in average drift using LADFN, while with filtering disabled, the drift in *Vanilla Stanley* is often so high that it leads to collision. This is not the case with LADFN which remains relatively unaffected, even with filtering disabled. It should also be noted that the impact of dynamic vehicles and feature-proximity on benchmark competitors gets pronounced as the LIDAR range decreases, while LADFN is resilient to these changes in LIDAR range.

The second column and the third column show the final drift and the final yaw offset at the end of the run respectively. They give an idea of the goal-reaching capabilities of all the approaches along with an intuition of how bad the future trajectory would be affected if the run was continued. We see that LADFN outperforms the benchmarks here with similar patterns as in column 1.

V. CONCLUSION

Future autonomous vehicles must actively navigate to reduce their localization and perception errors as well as optimize for conventional metrics such as obstacle avoidance and time-efficient navigation. This paper presents a principled method, based on deep RL, to synthesize navigation behaviors that significantly reduce localization error for autonomous vehicles using state-of-the-art LIDAR SLAM methods. Our key technical insight was to adopt a hierarchical RL approach, which focuses on selecting drift-minimizing waypoints that can be efficiently tracked by a low-level Stanley Controller [4].

In future work, we plan to implement our perception-aware RL navigation algorithm on a small mobile robot that operates in crowded, dynamic scenes. Moreover, we plan to work towards theoretical guarantees based on a model predictive control (MPC) framework where a robot must jointly optimize for safe, time-optimal waypoint control as well as minimizing localization errors.

REFERENCES

- [1] A. Dosovitskiy, G. Ros, F. Codevilla, A. Lopez, and V. Koltun, "CARLA: An open urban driving simulator," in *Proceedings of the 1st Annual Conference on Robot Learning*, 2017, pp. 1–16.
- [2] J. Zhang and S. Singh, "Loam: Lidar odometry and mapping in real-time," in *Robotics: Science and Systems*, vol. 2, no. 9, 2014.
- [3] J. Schulman, F. Wolski, P. Dhariwal, A. Radford, and O. Klimov, "Proximal policy optimization algorithms," *arXiv preprint arXiv:1707.06347*, 2017.
- [4] G. M. Hoffmann, C. J. Tomlin, M. Montemerlo, and S. Thrun, "Autonomous automobile trajectory tracking for off-road driving: Controller design, experimental validation and racing," in *2007 American Control Conference*, 2007, pp. 2296–2301.
- [5] F. Dellaert and M. Kaess, "Square root sam: Simultaneous localization and mapping via square root information smoothing," *The International Journal of Robotics Research*, vol. 25, no. 12, pp. 1181–1203, 2006.
- [6] M. Kaess, A. Ranganathan, and F. Dellaert, "isam: Incremental smoothing and mapping," *IEEE Transactions on Robotics*, vol. 24, no. 6, pp. 1365–1378, 2008.
- [7] B. Kitt, A. Geiger, and H. Lategahn, "Visual odometry based on stereo image sequences with ransac-based outlier rejection scheme," in *Intelligent Vehicles Symposium (IV)*, 2010.
- [8] T. Shan and B. Englot, "Lego-loam: Lightweight and ground-optimized lidar odometry and mapping on variable terrain," in *2018 IEEE/RSJ International Conference on Intelligent Robots and Systems (IROS)*. IEEE, 2018, pp. 4758–4765.
- [9] M. Labbé and F. Michaud, "Rtab-map as an open-source lidar and visual simultaneous localization and mapping library for large-scale and long-term online operation," *Journal of Field Robotics*, vol. 36, no. 2, pp. 416–446, 2019.
- [10] R. Mur-Artal, J. M. M. Montiel, and J. D. Tardos, "Orb-slam: a versatile and accurate monocular slam system," *IEEE transactions on robotics*, vol. 31, no. 5, pp. 1147–1163, 2015.
- [11] Y. Wang and S. Huang, "Towards dense moving object segmentation based robust dense rgb-d slam in dynamic scenarios," in *2014 13th International Conference on Control Automation Robotics & Vision (ICARCV)*. IEEE, 2014, pp. 1841–1846.
- [12] D.-H. Kim and J.-H. Kim, "Effective background model-based rgb-d dense visual odometry in a dynamic environment," *IEEE Transactions on Robotics*, vol. 32, no. 6, pp. 1565–1573, 2016.
- [13] Y. Sun, M. Liu, and M. Q.-H. Meng, "Improving rgb-d slam in dynamic environments: A motion removal approach," *Robotics and Autonomous Systems*, vol. 89, pp. 110–122, 2017.
- [14] B. Bescos, J. M. Fàcil, J. Civera, and J. Neira, "DynaSLAM: Tracking, mapping, and inpainting in dynamic scenes," *IEEE Robotics and Automation Letters*, vol. 3, no. 4, pp. 4076–4083, 2018.
- [15] R. Scona, M. Jaimez, Y. R. Petillot, M. Fallon, and D. Cremers, "Staticfusion: Background reconstruction for dense rgb-d slam in dynamic environments," in *2018 IEEE International Conference on Robotics and Automation (ICRA)*. IEEE, 2018, pp. 3849–3856.
- [16] Y. Sun, M. Liu, and M. Q.-H. Meng, "Motion removal for reliable rgb-d slam in dynamic environments," *Robotics and Autonomous Systems*, vol. 108, pp. 115–128, 2018.
- [17] J. Cheng, C. Wang, and M. Q.-H. Meng, "Robust visual localization in dynamic environments based on sparse motion removal," *IEEE Transactions on Automation Science and Engineering*, vol. 17, no. 2, pp. 658–669, 2019.
- [18] A. Kundu, K. M. Krishna, and C. Jawahar, "Realtime multibody visual slam with a smoothly moving monocular camera," in *2011 International Conference on Computer Vision*. IEEE, 2011, pp. 2080–2087.
- [19] N. D. Reddy, P. Singhal, V. Chari, and K. M. Krishna, "Dynamic body vslam with semantic constraints," in *2015 IEEE/RSJ International Conference on Intelligent Robots and Systems (IROS)*. IEEE, 2015, pp. 1897–1904.
- [20] F. Pomerleau, P. Krüsi, F. Colas, P. Furgale, and R. Siegwart, "Long-term 3d map maintenance in dynamic environments," in *2014 IEEE International Conference on Robotics and Automation (ICRA)*. IEEE, 2014, pp. 3712–3719.
- [21] D. Sun, F. Geißer, and B. Nebel, "Towards effective localization in dynamic environments," in *2016 IEEE/RSJ International Conference on Intelligent Robots and Systems (IROS)*. IEEE, 2016, pp. 4517–4523.
- [22] D. Fox, W. Burgard, and S. Thrun, "Active markov localization for mobile robots," *Robotics and Autonomous Systems*, vol. 25, no. 3–4, pp. 195–207, 1998.
- [23] N. Roy, W. Burgard, D. Fox, and S. Thrun, "Coastal navigation-mobile robot navigation with uncertainty in dynamic environments," in *Proceedings 1999 IEEE International Conference on Robotics and Automation (Cat. No. 99CH36288C)*, vol. 1. IEEE, 1999, pp. 35–40.
- [24] G. Dudek, K. Romanik, and S. Whitesides, "Localizing a robot with minimum travel," *SIAM Journal on Computing*, vol. 27, no. 2, pp. 583–604, 1998.
- [25] M. Rao, G. Dudek, and S. Whitesides, "Minimum distance localization for a robot with limited visibility," in *Proceedings of the 2005 IEEE International Conference on Robotics and Automation*. IEEE, 2005, pp. 2438–2445.
- [26] S. Bhuvanagiri and K. M. Krishna, "Motion in ambiguity: Coordinated active global localization for multiple robots," *Robotics and Autonomous Systems*, vol. 58, no. 4, pp. 399–424, 2010.
- [27] H. Durrant-Whyte and T. Bailey, "Simultaneous localization and mapping: part i," *IEEE robotics & automation magazine*, vol. 13, no. 2, pp. 99–110, 2006.
- [28] A. Geiger, P. Lenz, and R. Urtasun, "Are we ready for autonomous driving? the kitti vision benchmark suite," in *Conference on Computer Vision and Pattern Recognition (CVPR)*, 2012.
- [29] A. Raffin, A. Hill, M. Ernestus, A. Gleave, A. Kanervisto, and N. Dormann, "Stable baselines3," <https://github.com/DLR-RM/stable-baselines3>, 2019.
- [30] A. Sakai, D. Ingram, J. Dinius, K. Chawla, A. Raffin, and A. Paques, "Pythonrobotics: a python code collection of robotics algorithms," *arXiv preprint arXiv:1808.10703*, 2018.
- [31] Q. M. Thomas, O. Wasenmüller, and D. Stricker, "Delio: Decoupled lidar odometry," in *2019 IEEE Intelligent Vehicles Symposium (IV)*. IEEE, 2019, pp. 1549–1556.
- [32] S. Zhao, Z. Fang, H. Li, and S. Scherer, "A robust laser-inertial odometry and mapping method for large-scale highway environments," in *2019 IEEE/RSJ International Conference on Intelligent Robots and Systems (IROS)*. IEEE, 2019, pp. 1285–1292.
- [33] A. Milioto, I. Vizzo, J. Behley, and C. Stachniss, "Rangenet++: Fast and accurate lidar semantic segmentation," in *2019 IEEE/RSJ International Conference on Intelligent Robots and Systems (IROS)*. IEEE, 2019, pp. 4213–4220.